Plasmonics (2011) 6:67–73
DOI 10.1007/s11468-010-9170-7

Direct Synthesis of Vertically Interconnected 3-D Graphitic Nanosheets on Hemispherical Carbon Particles by Microwave Plasma CVD

Jitendra N. Tiwari · Rajanish N. Tiwari · Gyan Singh · Kun-Lin Lin

Received: 15 July 2010 / Accepted: 1 October 2010 / Published online: 12 October 2010

Abstract High-quality, free-standing, and vertically interconnected three-dimensional (3-D) graphitic nanosheets (GNSs) were synthesized over the surface of hemispherical carbon particles/GaN at 700 °C by microwave plasma chemical vapor deposition (CVD) in presence of methane gas, whereas the hemispherical carbon particles have been directly deposited on GaN/sapphire template. The GNSs are ~1–5 nm in thickness and have a graphitic flake structure on hemispherical carbon particles. The vertically interconnected 3-D GNSs on hemispherical carbon particles have been characterized by scanning electron microscopy, transmission electron microscopy, selective area electron diffraction pattern, X-ray diffraction, atomic force microscopy, Raman spectroscopy, X-ray photoelectron spectroscopy, and nitrogen gas adsorption-Brunauer-Emmet-Teller. The present CVD approach is capable of producing large quantities of GNSs with high purity. Moreover, a high-purity free-standing and vertically interconnected 3-D GNSs on hemispherical carbon particles have an enormous potential for applications in electronic devices, biological sensors, gas uptake and storage, fuel cells, lithium ion batteries, and more.

Keywords Microwave plasma CVD · Graphitic nanosheets · Electron microscopy · Surface properties

J. N. Tiwari (✉) · R. N. Tiwari
Department of Materials science and Engineering,
National Chiao Tung University,
1001 Ta Hsueh Road,
Hsinchu, Taiwan 300, Republic of China
e-mail: jnt_tiw123@yahoo.co.in

G. Singh
Department of Biological Science and Technology,
National Chiao Tung University,
1001 Ta Hsueh Road,
Hsinchu, Taiwan 300, Republic of China

K.-L. Lin
Department of Mechanical Engineering,
National Taiwan University of Science and Technology,
Taipei, Taiwan 0660, Republic of China

Introduction

Over the last decade, the advanced properties and applications of fullerenes, nanotubes, and nanofibers have been well accepted. However, allotrope of carbon such as graphite, characterized by its nanoscale thickness and open geometry (large specific surface-to-volume ratio and sharp edges), has not been thoroughly investigated. The graphitic nanosheets (GNSs) with a few nanometers thick may have a wide-range applications, for example serving as catalyst supports [1, 2], electrode materials for lithium ion batteries [3], and conductive fillers for conducting polymer composites [4–6], because of their remarkable surface area as well as special characteristics of flexibility and elasticity, high thermal resistance, high chemical stability, and light weight [7]. In addition, such two-dimensional (2-D) nanostructured materials may serve as the building blocks for other promising carbon materials. For example, nanotube-like carbon nanoscrolls have been formed from exfoliated graphite nanosheets via a scrolling mechanism [8], carbon nanohorns are a new type of horn-shaped aggregate of single-walled graphene sheets [9], and carbon nanowalls could be in nature regarded as well-separated graphene sheets vertically growing on the substrates [10].

Free-standing and vertically interconnected three-dimensional (3-D) graphite sheets could serve as an ideal material for catalyst support or an efficient edge emitter for electron field emission. Isolated, sheet/petal-like graphitic

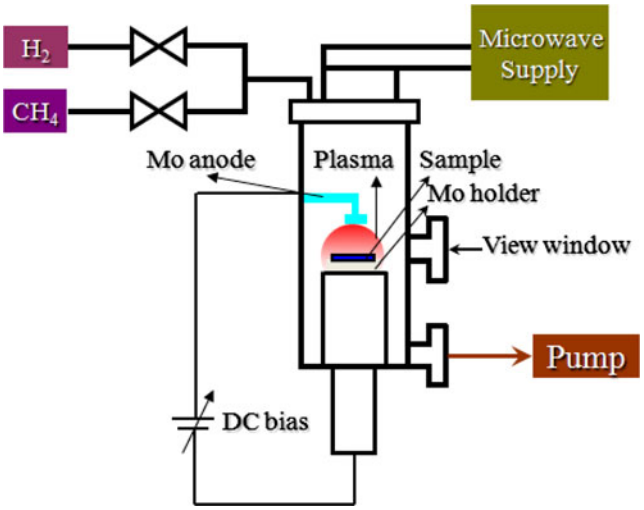

Fig. 1 Schematic of the microwave plasma CVD system for the growth of GNSs

structures were previously reported as byproducts during fullerene and nanotube preparations by arc-discharge method [11–13] and laser ablation [13]. However, in all cases, the produced GNSs coexisted with other carbon forms and had very low controllability. Many efforts were afterwards made to get GNSs, but only low yield of GNSs were achieved. Therefore, the synthesis of GNSs with high yield has been a challenge for researchers in recent years.

Herein, we report for the first time the synthesis of free-standing and vertically interconnected 3-D GNSs on hemispherical carbon particles. Microwave plasma chemical vapor deposition (CVD) has been used to synthesize the ~1–5-nm-thick GNSs in absence of catalyst or any substrate pretreatment and their basic properties were studied. The vertically interconnected 3-D GNSs synthesized by this proposed method have excellent specific surface area with high open surface. Moreover, the preparation method is controllable and can be used to produce GNSs with high yield. We believe that our findings represent an important development in the preparation of high-quality 3-D GNSs on a large scale, which may significantly facilitate the application of GNSs in a wide range of areas.

Experimental Methods

Free-standing and vertically interconnected 3-D GNSs on hemispherical carbon particles have been successively synthesized on GaN/sapphire template. The synthesis was carried out in a 2.45-GHz ASTeX type microwave plasma CVD system as shown in Fig 1. We have optimized the experimental conditions needed for the successive formation of hemispherical carbon particles and 3-D GNSs over it. In order to optimize the microwave discharge and the extension of the bias discharge over the entire substrate, we used a dome-shaped Mo anode which was placed above the substrate as counter-electrode. The ~3 μm thickness of GaN has been formed on sapphire substrate by metal-organic CVD. Prior to the deposition hemispherical carbon particles and GNSs over it, the template was ultrasonically cleaned with acetone and alcohol for 12 min each. For carburization of template, 4% CH_4 at a pressure of 20 torr and microwave power at 550 W has been used. For the deposition of hemispherical carbon particles and GNSs over it, we used 2.9% CH_4 at a pressure of 40 torr with 800 W applied microwave power and bias voltage of −100 V for 30 min and followed by further deposition for ~2 h without bias to the template. The 3-D GNSs on hemispherical carbon particles were analyzed by a standard X-ray diffractometer (XRD) with a Cu Kα source. Atomic force microscopy (AFM) was carried out to study the thickness (layer number) of GNS dispersed on silicon substrate. The microstructure of the 3-D GNSs on hemispherical carbon particles were evaluated with Raman microscopy (LABRAMHR).

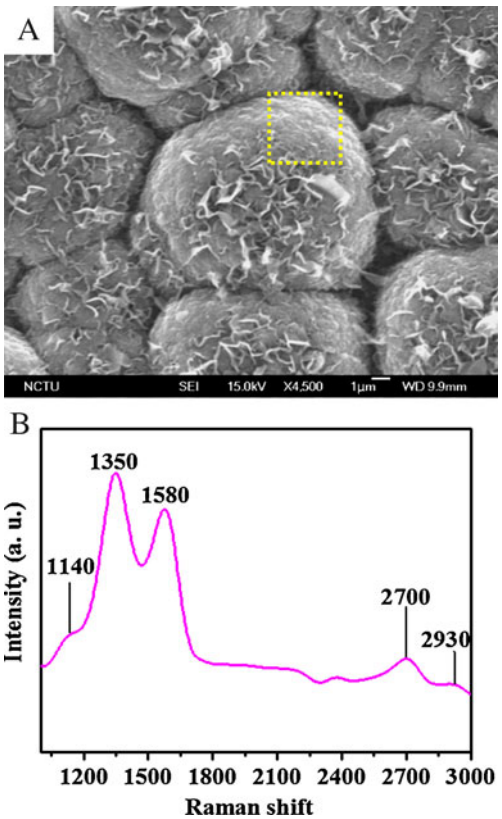

Fig. 2 **a** SEM image of partially etched GNSs on hemispherical carbon particles and **b** Raman spectra of selected region of the hemispherical particle shown in Fig. 1a

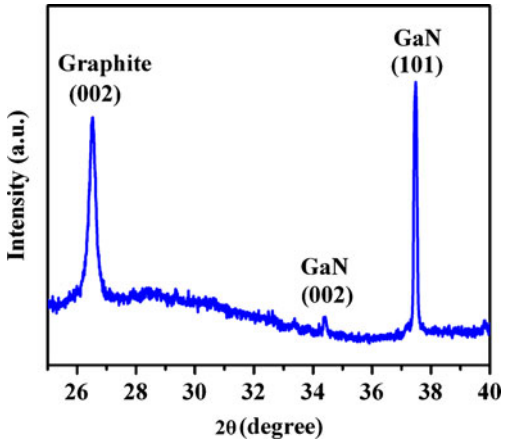

Fig. 3 XRD pattern of the GNSs on hemispherical carbon particles

Results and Discussion

The vertically interconnected 3-D GNSs grown on hemispherical particles was scratched off after treatment with ethanol to obtain the partially covered GNSs hemispherical particles. The surface morphology of the hemispherical particles was then examined by using field-emission scanning electron microscopy (FESEM, JEOL JSM-6700 F). Figure 2a shows the SEM image of the partially covered GNSs hemispherical particles. We select the non-covered GNSs region on hemispherical particle to study the chemical bonds of hemispherical particles, which play a major role in the growth of vertically interconnected GNSs.

It is well known that the all the forms of carbon materials such as amorphous carbon, fullerenes, carbon nanotubes, polycrystalline carbon etc. have been characterized by Raman spectroscopy. The positions of spectral bands are governed by the nature of the chemical bonds of carbon. Therefore, the Raman spectrum may provide additional information about the as-prepared partially covered GNSs hemispherical particles. Figure 2b shows a typical Raman spectrum taken from the marked area of hemispherical particle shown in Fig. 2a. As shown in Fig. 2b, there are three strong peaks at 1,350, 1,580, and 2,700 cm^{-1}, corresponding to D, G, and 2D bands of microcrystalline graphite, respectively. The intensity of the D band is stronger than that of the G band for hemispherical carbon structures, revealing that the hemispherical carbon particles

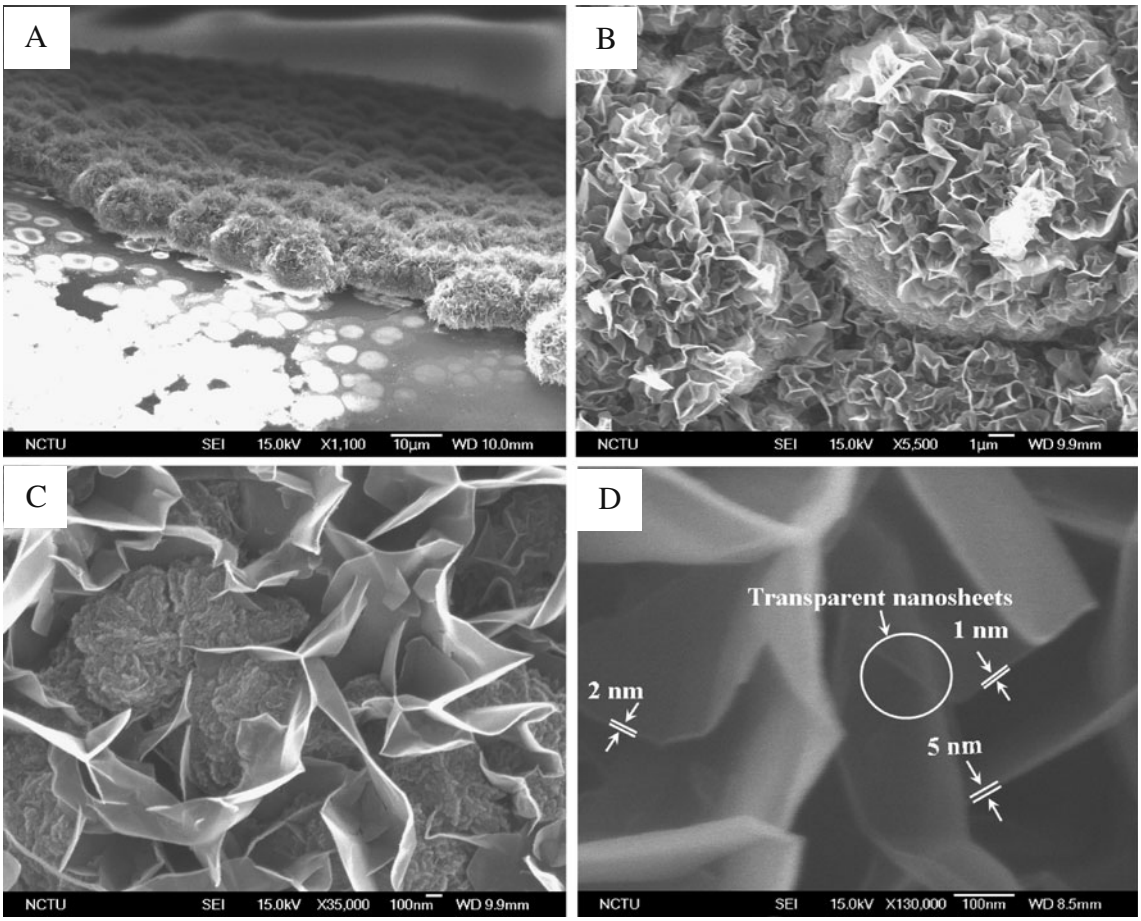

Fig. 4 **a** Side view FESEM image of the GNSs on hemispherical carbon particles; and **b**–**d** plane view FESEM images of the GNSs on hemispherical carbon particles at different magnifications

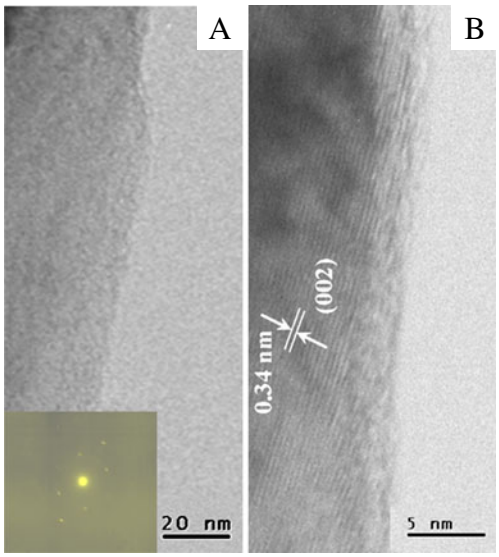

Fig. 5 **a** TEM image of the individual GNS and the corresponding SAED pattern is shown in the *inset*, and **b** HRTEM of the individual GNS

are less graphitized. A weak peak at 2,930 cm^{-1} can be assigned to the D+G bands of microcrystalline graphite [14]. A small broad peak at 1,140 cm^{-1} was observed in Raman spectra that correspond to the non-translational symmetric sp^3 phase in nanodiamond [15]. From Raman results, we confirmed that the hemispherical particles behind the GNSs were composed of carbon.

The phase structure of the as-prepared final product was characterized by XRD. Figure 3 shows a typical XRD pattern of the as-prepared 3-D GNSs on hemispherical carbon particles. A sharp and intense XRD diffraction peak at about $2\theta=26.6°$ can be indexed as the (002) diffraction reveals the high-quality graphitic nature of nanosheets. The weak and very sharp peaks at about $2\theta=34.8°$ and $2\theta=37°$ could be due to the GaN substrate and these two diffraction peaks are corresponding to (002) and (101) planes, respectively. The interlayer spacing (d) is calculated using Bragg equation:

$$d = \lambda/2\sin\theta_B$$

where $\lambda=1.54$ Å and θ_B is the corrected angle (Bragg angle) of incidence for the Cu Kα radiation. The interlayer spacing is calculated to be ~0.34 nm from the position of (002) reflection peak are similar to those observed for bulk hexagonal graphite (~0.335 nm) [16]. Later on, high-resolution transmission electron microscope (HRTEM) analysis was performed to confirm the interlayer spacing.

Further, the morphology of the 3-D GNSs on hemispherical carbon particles obtained under typical synthesis conditions were examined by using FESEM, transmission electron microscope (Philips TEM), selected-area electron diffraction (SAED), and HRTEM. Figure 4a–d shows the typical FESEM images of the product prepared by microwave plasma CVD in presence of methane/hydrogen

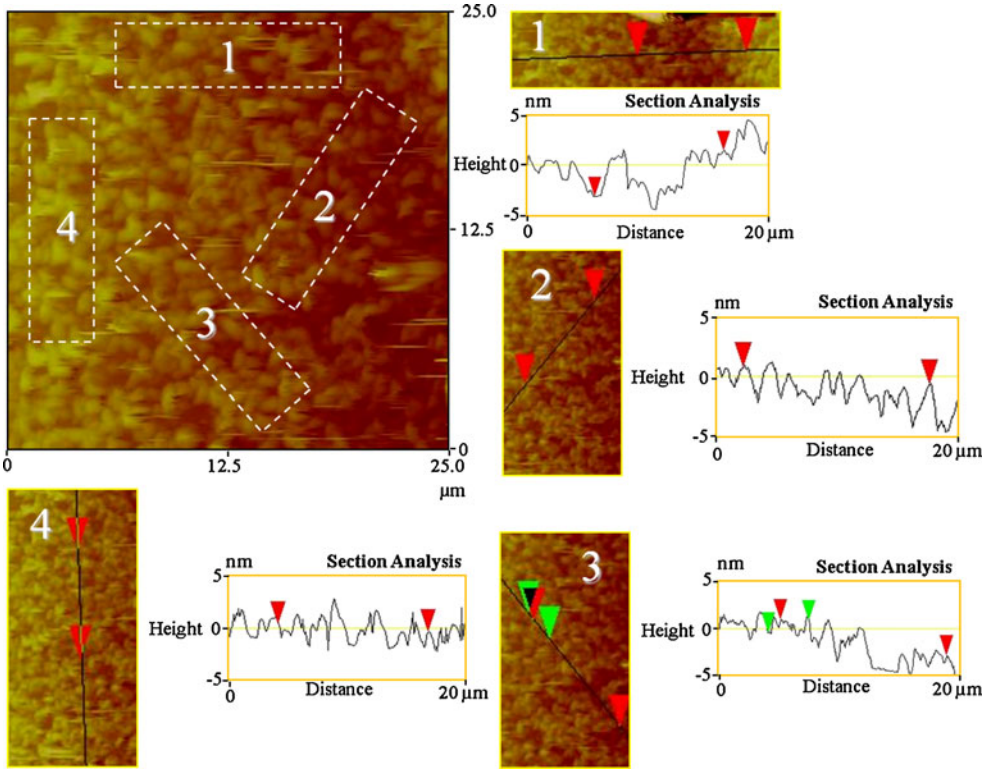

Fig. 6 AFM image of GNSs containing two layers (regions *2* and *4*) and 3–4 layers (region *1* and *3*) on silicon substrate

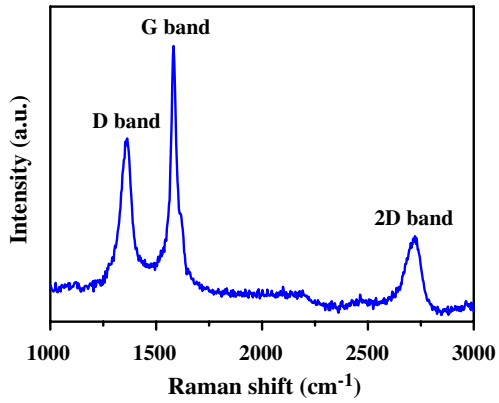

Fig. 7 Raman spectrum of the GNSs

gas mixture. Figure 4a and b show the low-resolution side view and plane view FESEM images of the 3-D GNSs on hemispherical carbon particles. As shown in the FESEM image in Fig. 4a, the as-obtained 3-D GNS consists of hemisphere carbon particles with diameters ranging from 9 to 10 μm. The magnified FESEM images (Fig. 4b) shows that the surfaces of hemispheres are not smooth. And the hemi-microspheres look like completely covered by the 3-D GNSs. Figure 4c shows the high-resolution FESEM image of 3-D GNSs on hemispherical carbon particle. The magnified FESEM image (Fig. 4c) clearly reveals that the 3-D GNSs on hemispherical carbon particles had a vertically interconnect structure.

On the basis of the image of morphology variation, a possible growth mechanism of vertically interconnect 3-D GNSs on hemispherical carbon particles can be explain in three steps. In first step, the particles are grown via stages of nucleation and growth, where nanoparticles are created within very short time by the various interactions between species at atomic and molecular levels. In addition, due to applied negative bias the nucleation density is also significantly increases. In second step, the particle in plasma are negatively charged due to bombardment of

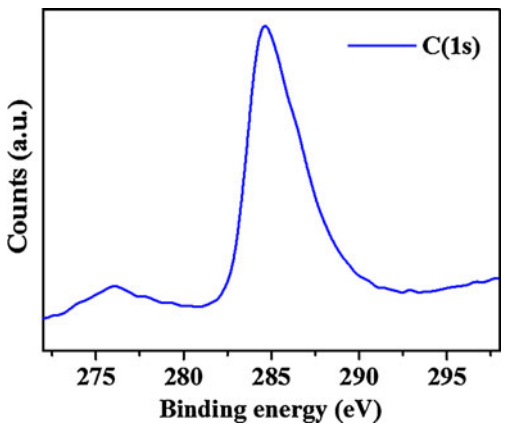

Fig. 8 XPS spectrum of the GNSs

high-energy electrons which are accelerated by the electric field in the sheath space after being ejected from the substrate surface under the energetic ionic bombardments, and as the result, the existing particles becomes positively charged [17, 18]. Therefore, it can be supposed that the motion of charged and uncharged carbon in the plasma plays an important role in the growth of large spherical carbon particles. Consequently, large hemispherical carbon particles are formed. In the final step, GNSs are formed, in this step the C_2 (C–C bond) bonds from the initially formed hemispherical carbon structures are connected linearly with each other. In addition, the free carbons from the plasma atmosphere will further adhere on the existing structure to become scale-like GNSs. The GNSs are then connected with each other in wavy fashion to become free-standing vertically interconnect GNSs. Although it is at present not clear exactly how the 3-D vertically interconnected GNSs and the hemispherical carbon particles form during the CVD growth, studies are underway to explore the detailed formation mechanism.

Figure 4d shows the high-resolution SEM image of the 3-D GNSs on hemispherical carbon particles. According to Fig. 4d, transparent individual graphite clearly overlaps on the hind GNS. The higher magnification FESEM image (Fig. 4d) clearly reveals that the GNSs have a thickness range 1 to 5 nm. But, we believed that the SEM image will not give the accurate thickness information of the GNSs. Therefore, the thickness of the GNSs was successfully confirmed by atomic force microscope, as shown later.

Figure 5a and b show the TEM image of an individual GNS and its corresponding SAED pattern with the electron beam directed along the individual GNS. The SAED pattern from the individual GNS shows few bright spots. The clearly visible bright spots confirm that the GNSs are single crystals. The HRTEM image taken at the top edge of the individual GNS shows that the interlayer distance about ~0.34 nm, as shown in Fig. 5b. The lattice spacing of ~0.34 nm corresponds to the (002) plane. This result is consistent with XRD data.

To gain the more insight into GNSs, we performed detailed AFM scans of GNSs dispersed on Si substrate. Analysis of a large number of AFM images in different regions revealed that the most of GNSs had thickness in the range of ~1 to ~5 nm, as

Table 1 Specific surface area for as-prepared GNSs and other carbon materials

Carbon material	References	A_{BET} ($m^2 g^{-1}$)
GNSs	Our sample	100.5
Natural graphite	[38]	1.7–6.0
Expanded graphite	[39]	40–60
Carbon sheets	[40]	97.2

shown in Fig. 6. Notably, about 90% of the GNSs had a uniform thickness. The thickness of the GNSs was calculated to be about ~1 nm (region 2 and 4 in Fig. 6), which is consistent with the thickness of a two layer graphene. On the other hand, the thickness of the GNSs was measured to be about more than ~2 nm (region 1 and 3 in Fig. 6), which is consistent with the thickness of a 3–6-layer graphene.

Further, we have investigated the degree of graphitization of GNSs by Raman spectroscopy. Raman spectra taken on GNSs, as shown in Fig. 6, are similar to those observed for graphitic carbon [19]. Second-order modes in the range of 2,000–3,000 cm^{-1} are also present in Fig. 7. Figure 7 shows that it has two strong peaks at 1,363, and 1,582 cm^{-1}. The peak at around 1,363 cm^{-1} is the D-band associated with vibrations of carbon atoms with dangling bonds in plane terminations of the disordered graphite. The peak at 1,582 cm^{-1} (G band) is attributed to the vibration of sp^2-bonded carbon atoms in a two-dimensional hexagonal lattice [20, 21]. Figure 7 also shows that the strong peak at about 2,716 cm^{-1}, is attributed to the disorder mode 2D band. From Fig. 7, we can see that the G-band peak is stronger than the D-band peak and their intensity ratio is about 1.4, unambiguously suggests that the 3-D GNSs have high degree of graphitization. In addition, the area ratio between the two bands (A_D/A_G) allows the degree of ordering or graphitization of the carbon structure to be characterized [22, 23]. In the spectra of highly crystalline graphite, D band is absent, which indicates the 100% degree of graphitization. It should be noted that the A_D/A_G value of GNSs (1.02) was smaller than that of Vulcan XC-72 and AP-carbon [24]. Furthermore, a similar value of A_D/A_G between GNSs (1.02) and MWCNT (1.03) [24] confirms that the 3-D GNSs retained similar graphitic characteristics to the MWCNT. The HRTEM image showing the 3-D GNSs (Fig. 4b) retained graphitic layers, also supporting the graphitic nature of GNSs.

X-ray photoelectron spectroscopy (XPS) is another powerful tool to investigate the different forms of carbon species. Hence, XPS was used to characterize the surface properties of the GNSs. Figure 8 shows the core level C(1s) spectra recorded for the as-prepared 3-D GNSs on hemispherical carbon particles. The XPS spectrum of synthesized 3-D GNSs has sharp peak at 284.6 eV, quit similar peak attributed to C = C graphitic species has been reported earlier [25]. In addition, no peaks appear at higher binding energies, i.e., peaks due to C–O species (286.6 eV), C = O species (287.9 eV), or the defect sp^3 C–C species (286.6 eV) [26, 27]. This implies the synthesized GNSs are highly pure graphitic structure. These results are consistent to Raman and XRD which confirms that the synthesized 3-D GNSs are high quality.

Finally, we measure the specific surface area of the 3-D GNSs on hemispherical carbon particles by nitrogen gas adsorption—BET (Brunauer-Emmet-Teller). The 3-D GNSs on hemispherical carbon particles obtained had BET surface areas of 100.5 m^2g^{-1} without activation. Therefore, the 3-D GNSs/hemispherical carbon particles will be very useful as a catalyst support [28], electronic devices [29], biological sensors [30], hydrogen gas sensor [31], gas uptake and storage [32], fuel cells [33–35], lithium ion batteries [36], and supercapacitor [37] through the high specific surface area. This is tens of times that of natural graphite [38] and two times higher than that of ordinary EG sheets [39] as well as much higher than that of crumpled carbon nanosheets [40] (data are listed in Table 1). Compared with other carbon materials, the specific surface area of as-prepared graphitic structures is relatively high. Thus, we conclude that the free-standing and vertically interconnected 3-D GNSs on hemispherical carbon particles with high purity, crystallinity, and excellent surface area could be obtained with such a facile CVD method.

Conclusions

In summary, we have reported for the first time, the synthesis of vertically interconnected three-dimensional graphitic nanosheets (GNSs, thickness in the range of 1 to 5 nm) on hemispherical carbon particles. The syntheses of vertically interconnected 3-D GNSs on hemispherical carbon particles have a large specific surface area and provide an avenue for potential applications in many areas as a catalyst support, biological sensors, electron devices, gas uptake and storage, fuel cells, lithium ion batteries, and so on. Moreover, the preparation method is controllable and can be used to produce GNSs in high yield. We believe that our findings represent an important development in the preparation of high-quality GNSs on a large scale.

Acknowledgments The authors would like to thank Prof. Fu-Ming Pan for availing us all the necessary lab facility, chemical, and reagent.

References

1. Li Y, Tang L, Li J (2009) Preparation and electrochemical performance for methanol oxidation of pt/graphene nanocomposites. Electrochem Commun 11(4):846–849
2. Yoo E, Okata T, Akita T, Kohyama M, Nakamura J, Honma I (2009) Enhanced electrocatalytic activity of Pt subnanoclusters on graphene nanosheet surface. Nano Lett 9(6):2255–2259
3. Yoshio M, Wang H, Fukuda K, Umeno T, Abe T, Ogumi Z (2004) Improvement of natural graphite as a lithium-ion battery anode material, from raw flake to carbon-coated sphere. J Mater Chem 14(11):1754–1758
4. Pan XY, Yu ZZ, Ou YC, Hu GH (2000) A new process of fabricating electrically conducting nylon 6/graphite nanocomposites via intercalation polymerization. J Polym Sci Pol Phys 38 (12):1626–1633

5. Chen GH, Wu DJ, Weng WG, Yan WL (2001) Dispersion of graphite nanosheets in a polymer matrix and the conducting property of the nanocomposites. Polym Eng Sci 41(12):2148–2154
6. Chen GH, Wu DJ, Weng WG, Wu CL (2003) Exfoliation of graphite flake and its nanocomposites. Carbon 41(3):619–621
7. Manning TJ, Mitchell M, Stach J, Vickers T (1999) Synthesis of exfoliated graphite from fluorinated graphite using an atmospheric-pressure argon plasma. Carbon 37(7):1159–1164
8. Viculis LM, Mack JJ, Kaner RB (2003) A chemical route to carbon nanoscrolls. Science 299(5611):1361
9. Iijima S, Yudasaka M, Yamada R, Bandow S, Suenaga K, Kokai F, Takahashi K (1999) Nano-aggregates of single-walled graphitic carbon nano-horns. Chem Phys Lett 309(3–4):165–170
10. Wu YH, Qiao PW, Chong TC, Shen ZX (2002) Carbon nanowalls grown by microwave plasma enhanced chemical vapor deposition. Adv Mater 14(1):64–67
11. Ando Y, Zhao X, Ohkohchi M (1997) Production of petal-like graphite sheets by hydrogen arc discharge. Carbon 35(1):153–158
12. Ebbesen TW, Ajayan PM (1992) Large scale synthesis of carbon nanotubes. Nature 358(6383):220–222
13. Iijima S, Wakabayashi T, Achiba Y (1996) Structures of carbon soot prepared by laser ablation. J Phys Chem 100(14):5839–5843
14. Kawashima Y, Katagiri G (1995) Fundamentals, overtones, and combinations in the Raman spectrum of graphite. Phys Rev B 52 (14):10053–10059
15. Shroder RE, Nemanich RJ, Glass JT (1990) Analysis of the composite structures in diamond thin films by Raman spectroscopy. Phys Rev B 41(6):3738–3745
16. Zhang HB, Lin GD, Zhou ZH, Dong X, Chen T (2002) Raman spectra of MWCNTs and MWCNT-based H_2-adsorbing system. Carbon 40(13):2429–2436
17. Stoffels WW, Stoffels E, Ceccone G, Rossi F (1999) Laser-induced particle formation and coalescence in a methane discharge. J Vac Sci Technol A 17(6):3385–3393
18. Choi SJ, Kushner MJ (1993) The role of negative ions in the formation of particles in low-pressure plasmas. J Appl Phys 74 (2):853–861
19. Reich S, Thomsen C (2004) Raman spectroscopy of graphite. Phil Trans R Soc Lond A 362(1824):2271–2288
20. Liu JW, Shao MW, Chen XY, Yu WC, Liu XM, Qian YT (2003) Large-scale synthesis of carbon nanotubes by an ethanol thermal reduction process. J Am Chem Soc 125(27):8088–8089
21. Liu JW, Shao MW, Tang Q, Zhang SY, Qian YT (2003) Synthesis of carbon nanotubes and nanobelts through a medial-reduction method. J Phys Chem B 107(26):6329–6332
22. Kim P, Joo JB, Kim W, Kim J, Song IK, Yi J (2006) Graphitic spherical carbon as a support for a PtRu-alloy catalyst in the methanol electrooxidation. Catal Lett 112(3–4):213–218
23. Mnaldonao F, Moreno C, Rivera J, Hanzawa Y, Yamada Y (2000) Catalytic graphitization of carbon aerogels by transition metals. Langmuir 16(9):4367–4373
24. Joo JB, Kim YJ, Kim W, Kim P, Yi J (2008) Simple synthesis of graphitic porous carbon by hydrothermal method for use as a catalyst support in methanol electro-oxidation. Catalysis Commun 10(3):267–271
25. Paredes JI, Villar-Rodil S, Martı'nez-Alonso A, Tascon JMD (2008) Graphene oxide dispersions in organic solvents. Langmuir 24(19):10560–10564
26. Yang D-Q, Rochette J-F, Sacher E (2005) Controlled chemical functionalization of multiwalled carbon nanotubes by kiloelectronvolt argon ion treatment and air exposure. Langmuir 21 (18):8539–8545
27. Yang D-Q, Sacher E (2006) Carbon 1 s x-ray photoemission line shape analysis of highly oriented pyrolytic graphite: the influence of structural damage on peak asymmetry. Langmuir 22(3):860–862
28. Kou R, Shao Y, Wang D, Engelhard MH, Kwak JH, Wang J, Viswanathan VV, Wang C, Lin Y, Wang Y, Aksay IA, Liu J (2009) Enhanced activity and stability of Pt catalysts on functionalized graphene sheets for electrocatalytic oxygen reduction. Electrochem Commun 11(5):954–957
29. Wei D, Liu Y, Wang Y, Zhang H, Huang L, Yu G (2009) Synthesis of N-doped graphene by chemical vapor deposition and its electrical properties. Nano Lett 9(5):1752–1758
30. Mohanty N, Berry V (2008) Graphene-based single-bacterium resolution biodevice and DNA transistor: interfacing graphene derivatives with nanoscale and microscale biocomponents. Nano Lett 8(12):4469–4476
31. Kaniyoor A, Jafri RI, Arockiadoss T, Ramaprabhu S (2009) Nanostructured Pt decorated graphene and multi walled carbon nanotube based room temperature hydrogen gas sensor. Nanoscale 1(3):382–386
32. Lv W, Tang DM, He YB, You CH, Shi ZQ, Chen XC, Chen CM, Hou PX, Liu C, Yang QH (2009) Low-temperature exfoliated graphenes: vacuum-promoted exfoliation and electrochemical energy storage. ACS Nano 3(11):3730–3736
33. Stolyarova E, Stolyarov D, Bolotin K, Ryu S, Liu L, Rim KT, Eom D, Klima M, Hybertsen M, Pogorelsky I, Pavlishin I, Kusche K, Hone J, Kim P, Stormer HL, Yakimenko V, Flynn G (2009) Observation of graphene bubbles and effective mass transport under graphene films. Nano Lett 9(1):332–337
34. Tiwari JN, Tiwari RN, Chang Y-M, Lin K-L (2010) A promising approach to the synthesis of 3D nanoporous graphitic carbon as a unique electrocatalyst support for methanol oxidation. ChemSusChem 3(4):460–466
35. Tiwari JN, Pan F-M, Chen T-M, Tiwari RN, Lin K-L (2010) Electrocatalytic activity of Pt nanoparticles electrodeposited on amorphous carbon-coated silicon nanocones. J Power Sources 195 (3):729–735
36. Yoo E, Kim J, Hosono E, Zhou H, Kudo T, Honma I (2008) Large reversible Li storage of graphene nanosheet families for use in rechargeable lithium ion batteries. Nano Lett 8(8):2277–2282
37. Wang Y, Shi Z, Huang Y, Ma Y, Wang C, Chen M, Chen Y (2009) Supercapacitor devices based on graphene materials. J Phys Chem C 113(30):13103–13107
38. Sato Y, Hagiwara R, Ito Y (2003) Refluorination of pyrocarbon prepared from fluorine—GIC. Solid State Sci 5(9):1285–1290
39. Celzard A, Mareche JF, Furdin G (2002) Surface area of compressed expanded graphite. Carbon 40(14):2713–2718
40. Kuang Q, Xie SY, Jiang ZY, Zhang XH, Xie ZX, Huang RB, Zheng LS (2004) Low temperature solvothermal synthesis of crumpled carbon nanosheets. Carbon 42(8–9):1737–1741